IEEE Access
Multidisciplinary | Rapid Review | Open Access Journal

Received October 6, 2017, accepted November 8, 2017, date of publication November 20, 2017,
date of current version December 22, 2017.

*Digital Object Identifier 10.1109/ACCESS.2017.2775210*

# A Simulation Framework for Multiple-Antenna Terminals in 5G Massive MIMO Systems

**ERIK L. BENGTSSON[1,2], FREDRIK RUSEK[2], STEFFEN MALKOWSKY[2], FREDRIK TUFVESSON[2], (Fellow, IEEE), PETER C. KARLSSON[1], AND OVE EDFORS[2]**

[1]Radio Access Lab, Sony Mobile Communications, SE221 88 Lund, Sweden
[2]Department of Electrical and Information Technology, Lund University, 221 00 Lund, Sweden

Corresponding author: Erik L. Bengtsson (erik.bengtsson@sony.com)

This work was supported in part by Sony Mobile Communications, Lund, and in part by Stiftelsen för Strategisk Forskning.

**ABSTRACT** The recent interest in massive multiple in multiple out (MIMO) has spurred intensive work on massive MIMO channel modeling in the contemporary literature. However, current models fail to take the characteristics of terminal antennas into account. There is no massive MIMO channel model available that can be used for the evaluation of the influence of different antenna characteristics at the terminal side. In this paper, we provide a simulation framework that fills this gap. We evaluate the framework with antennas integrated into Sony Xperia handsets operating at 3.7 GHz as this spectrum is identified for the 5G new radio standard by 3rd Generation Partnership Project. The simulation results are compared with the measured terminal performance when communicating with the Lund University's massive MIMO testbed under the same loading conditions. Expressions are derived for comparison of the gain obtained from different diversity schemes computed from measured far-field antenna patterns. We conclude that the simulation framework yields the results close to the measured ones and that the framework can be used for antenna evaluation for terminals in a practical precoded massive MIMO system.

**INDEX TERMS** Diversity, terminal antenna, massive multiple in multiple out (MIMO), 5G, NR, channel model, transmission scheme, pilot signal, SRS.

## I. INTRODUCTION

Massive multiple in multiple out (MIMO) (MaMi) technology [1] is emerging as one of the major candidates for increasing capacity and efficiency of future wireless communications systems [2]. Recent predictions show that MaMi can increase energy efficiency by several orders of magnitude and spectral efficiency by at least one order of magnitude, under reasonable assumptions on channel and system configurations [3]. Lately, world records in measured spectral efficiency have been reported [4]. The current one (145.6 bits/s/Hz) is more than 20 times what can be achieved with LTE Rel-10. The large gains have spurred various companies to promote MaMi as a component in the 3rd Generation Partnership Project new radio (NR) standard for the fifth generation wireless communication [5], [6]. Despite a frenetic research activity on MaMi, terminal antenna and RF configuration perspectives have been almost entirely neglected. One reason for the base station (BS) focus is that most new concepts relate to it and only indirectly to terminal devices. Terminal modems with baseband algorithms and antenna designs, however, influence overall performance to a large extent.

Notable exceptions to the BS focus are [7]–[9]. In [7] the impact of terminal hardware impairments on the achievable capacity, as the number of BS antennas grows large, is studied. Reference [8] deals with simulation of measured terminal far-field antenna patterns in MaMi multi-stream operation, and can be seen as a starting point of our work in this area. In [9] we conducted an initial measurement campaign and formulated a number of transceiver strategies for MaMi systems with multi-antenna terminals.

In this paper, we propose a simulation framework based on [8], including the transceiver strategies from [9], designed for evaluation of multi-antenna terminals. The framework avoids the complexity of a MaMi BS with its hundreds of antennas and a full geometric channel description, but still takes effects of terminal antenna patterns and BS precoding into account. We demonstrate the simulation framework performance under different terminal antenna loading conditions in combination with different transceiver strategies. Ideally MaMi can coherently combine signals associated with different propagation paths, thereby remove the small-scale fading. Therefore, the diversity schemes studied here target

large-scale fading caused by shadowing and antenna loading at the terminal side. Antennas have been integrated into commercially available smartphone chassis and tuned for operation in the 3.7 GHz band used by the Lund University MaMi (LuMaMi) testbed [10], [11]. Results provided by the simulation framework are compared to measurements obtained by using the same terminal in the LuMaMi testbed.

### A. PAPER CONTRIBUTIONS

The main contributions of this paper are that we

- derive a simulation framework for the evaluation of measured far-field antenna patterns from multi-antenna terminals, in a precoded MaMi system.
- match simulated and measured MaMi channel matrices by tuning only three environmental parameters.
- show that for a multi-antenna terminal, the chosen uplink pilot transmission strategy can give substantial SNR gains in the precoded downlink.
- evaluate the generality of the environmental parameters by the testing of a second terminal with a different antenna implementation. Antenna patterns from the second terminal are used in the simulation framework, with environmental settings derived for the first prototype. Finally, the simulated SNR gains and powers are compared to measured values.

Fig. 1 outlines our simulation approach and its inputs: a few environmental parameters and measured antenna patterns.

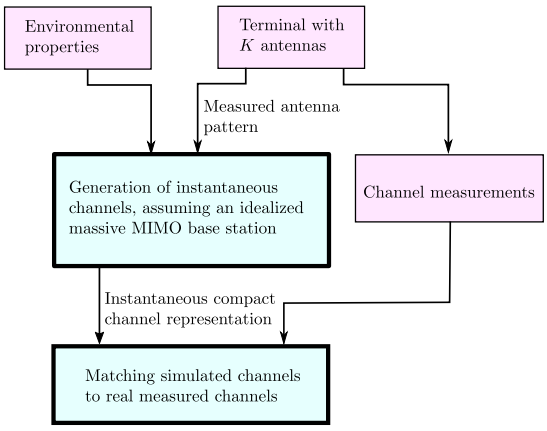


**FIGURE 1. Approach for the derivation of environmental properties. The environmental parameters and antenna patterns are inputs to the simulation framework, and the same antennas are measured in a real massive MIMO channel. The environmental parameters are changed so that the distribution of the compact channel representation match the measured ones.**

### B. PAPER ORGANIZATION

In Section II we briefly discuss channel models and motivate a cluster-based approach for the simulation framework. Section III presents the main contribution of this work, the simulation framework. In Section IV we tune environmental properties so that statistical properties of simulations match those of measured channels. In Section V we incorporate the different transceiver schemes from [9] to illustrate how the framework can be used. We derive expressions for received signal power where the transceiver schemes are reflected. Section VI presents the simulated power gains and compares to testbed measurements. A summary is provided in Section VII.

## II. CHANNEL MODELS

The most common narrowband signal model for wireless transmission in general, and for MaMi in particular, is

$$\boldsymbol{y} = \boldsymbol{H}\boldsymbol{x} + \boldsymbol{n}, \tag{1}$$

where $\boldsymbol{y} = [y_0\ y_1 \cdots y_{K-1}]^{\mathrm{T}}$ is the vector of signals at the feed of $K$ terminal receive antennas, and $\boldsymbol{x} = [x_0\ x_1 \cdots x_{2J-1}]^{\mathrm{T}}$ represents the signals fed to $J$ dual orthogonal polarized antenna elements (henceforth referred to as antenna elements) with 2 ports each, giving $2J$ antenna ports at the BS. $\boldsymbol{H}$ is a $K \times 2J$ matrix representing the radio channel and $\boldsymbol{n}$ the noise vector. In (1), each entry $h_{kj}$ in $\boldsymbol{H}$ represents the transfer function from a BS transmit antenna port $j$ to a terminal receive antenna $k$. These entries include antenna gains from the transmit and receive antennas, as well as the propagation channel gain considering all contributions along the different propagation paths, respectively. To evaluate the impact of different antenna configurations, we need to isolate the influence of the terminal antenna pattern on $h_{kj}$.

In [8], we used a Kronecker assumption [12] for evaluating different transceiver schemes. A shortcoming of the Kronecker model is the limited possibility to include directional properties of the antennas; handset antennas are influenced by the user in many scenarios, which changes directive properties of the antennas. The directional gain will also increase as multi-antenna terminals become more important to compensate for smaller apertures at higher frequencies, anticipated in [5] and [6]. Similarly, classic models assuming independent identically distributed (i.i.d.) signal contributions at the terminal side do not model the MaMi channel in a realistic manner and ignores directional properties [13]–[16]. Equivalently, the mean effective gain (MEG) [17], [18], a commonly used figure of merit for antennas, does not apply for MaMi. As the name implies, a mean of independent contributions is then considered. MaMi, on the other hand, has the capability to control phase, amplitude, and polarization of multiple signal contributions, that illuminate the terminal antennas and thus enable a coherent combination of them. This, in combination with channel hardening [19], makes the effective channel more deterministic. This points towards a need for new performance evaluation strategies.

To evaluate the impact of different antenna configurations and their directional properties, we must know the directional properties of the propagation channel. We use a cluster-based channel model in our simulation framework, thereby including directional properties naturally. Each entry $h_{kj}$ in $\boldsymbol{H}$ is a sum of contributions from $N$ clusters, as described in the channel model in Fig. 2. This enables us to include real measured antenna patterns and characterize the effective

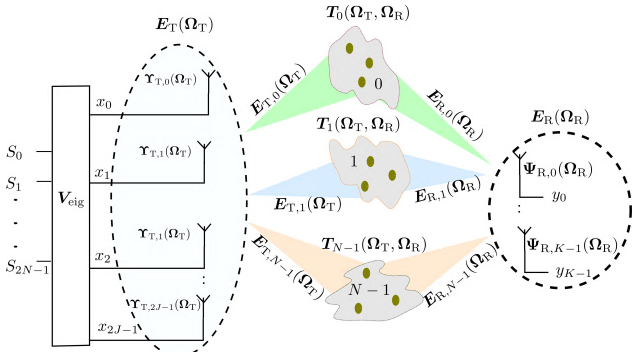


**FIGURE 2. Transmission from *J* BS transmit antennas to *K* closely spaced terminal receive antennas over *N* spatially separated clusters. Note that the variables in the figure are defined later in the text.**

precoded MaMi channel with a few environment dependent cluster parameters.

## III. DERIVATION OF THE SIMULATION FRAMEWORK

### A. A CLUSTER BASED PROPAGATION MODEL

A typical MaMi BS uses received uplink pilot signals (SRS in [6]) to obtain channel estimates, from which it determines terminal specific precoding vectors. For a detailed analysis of a given deterministic channel, one may evaluate different antenna configurations with full wave analysis. However, defining the complex E-field at the terminal side by linear combinations of transmitted signals from the BS side may limit the intuitiveness, and some simplifications can hence be convenient. Here we, with the help of well-motivated assumptions, model the propagation channel with only a few input parameters, still capturing the dominant propagation effects. The assumptions we make are the following:

1) All clusters are in the far field as seen from the antennas. By defining the antennas at the receiver side to have the same center points and similar for the transmit antennas, equations are greatly simplified as all antennas at each side will be exposed to the same electrical field. (Note that as a consequence, near field effects are not captured).
2) A cluster is defined by a center angle and an angular spread. The cluster gain function, and thus also the signal strength, of a cluster is constant within angles defined by the cluster.
3) The BS can individually control power level, phase, and polarization of the signal to each cluster seen by the BS.
4) The cluster gain does not depend on polarization as it does not favor any polarization direction.
5) The center angles of clusters are uniformly distributed, as seen by the terminal antennas.

We discuss the assumptions in greater detail and their consequences as we derive our framework next. We also refer back to these assumptions when we derive our expressions.

The angular resolution of an antenna array depends on the number of antennas. However, even with hundreds of antennas, we cannot assume that it is possible for a MaMi BS to resolve every individual multipath component (MPC) in the channel. Motivated by [20] and [21], we use $N$ clusters to represent signals from multiple propagation paths with similar illumination angles and propagation delays. Directional angles are represented by $\boldsymbol{\Omega} = [\Theta \ \ \Phi]^{\mathrm{T}}$ where $\Theta$ and $\Phi$ are elevation and azimuth angles, respectively, see Fig. 2. We use subscript R in $\boldsymbol{\Omega}_{\mathrm{R}}$ to define the AOA of the received signals at the terminal side and subscript T in $\boldsymbol{\Omega}_{\mathrm{T}}$ to define the AOD of the transmitted signals from the BS side.

The E-field $\boldsymbol{E}_{\mathrm{R}}(\boldsymbol{\Omega}_{\mathrm{R}})$, illuminating the terminal antennas, is a sum of $N$ contributions from the clusters, $\boldsymbol{E}_{\mathrm{R}}(\boldsymbol{\Omega}_{\mathrm{R}}) = \sum_{n=0}^{N-1} \boldsymbol{E}_{\mathrm{R}n}(\boldsymbol{\Omega}_{\mathrm{R}})$. The E-field generated by each cluster $\boldsymbol{E}_{\mathrm{R}n}(\boldsymbol{\Omega}_{\mathrm{R}}) = 0$ for $\boldsymbol{\Omega}_{\mathrm{R}} \notin \mathcal{A}_n$, where $\mathcal{A}_n$ is the set of AOAs illuminated by cluster $n$. Based on Assumption 1), all terminal antennas see the same E-field, and for terminal antenna $k$ this gives an output signal

$$y_k = \sum_{n=0}^{N-1} \int_{4\pi} \boldsymbol{\Psi}_k^{\mathrm{H}}(\boldsymbol{\Omega}_{\mathrm{R}}) \boldsymbol{E}_{\mathrm{R}n}(\boldsymbol{\Omega}_{\mathrm{R}}) \mathrm{d}\boldsymbol{\Omega}_{\mathrm{R}}, \tag{2}$$

where $\boldsymbol{\Psi}_k(\boldsymbol{\Omega}_{\mathrm{R}})$ is the gain function of terminal antenna $k$. Both $\boldsymbol{E}_{\mathrm{R}n}(\boldsymbol{\Omega}_{\mathrm{R}})$ and $\boldsymbol{\Psi}_k(\boldsymbol{\Omega}_{\mathrm{R}})$ are $2 \times 1$ vectors of functions where the entries represent the different polarizations along the respective angles, i.e., $\boldsymbol{\Psi}_k(\boldsymbol{\Omega}_{\mathrm{R}}) = [\Psi_k^{\Theta}(\boldsymbol{\Omega}_{\mathrm{R}}) \ \ \Psi_k^{\Phi}(\boldsymbol{\Omega}_{\mathrm{R}})]^{\mathrm{T}}$.

To model the properties of cluster $n$ we use a cluster transfer function $\boldsymbol{T}_n(\boldsymbol{\Omega}_{\mathrm{R}}, \boldsymbol{\Omega}_{\mathrm{T}})$, a $2 \times 2$ matrix, with entries for each polarization on the diagonal and cross polarization terms at the off-diagonals. The cluster transfer function couples the AOD at the BS transmit antennas to AOA at the terminal receive antennas and defines the cluster gain and phase properties.

Each BS antenna element has two orthogonal linearly polarized ports. The antenna patterns for both ports of the $j^{\mathrm{th}}$ antenna element are assembled into the $2 \times 2$ diagonal matrix,

$$\boldsymbol{\Upsilon}_j(\boldsymbol{\Omega}_{\mathrm{T}}) = \begin{bmatrix} \Upsilon_j^{\Theta}(\boldsymbol{\Omega}_{\mathrm{T}}) & 0 \\ 0 & \Upsilon_j^{\Phi}(\boldsymbol{\Omega}_{\mathrm{T}}) \end{bmatrix}. \tag{3}$$

As we assume far field conditions also at the BS side, all BS antennas see the same clusters. Like the terminal antennas, the BS antenna patterns are defined with a common center point. Hence, assuming that all elements have equal gain patterns, the physical distance between the antennas yields an AOD dependent phase offset in the signal.

We can express each element in the channel matrix $\boldsymbol{H}$ in (1) as a sum of contributions from the different clusters,

$$h_{kj} = \sum_{n=0}^{N-1} \int_{4\pi} \int_{4\pi} \boldsymbol{\Psi}_k^{\mathrm{H}}(\boldsymbol{\Omega}_{\mathrm{R}}) \boldsymbol{T}_n(\boldsymbol{\Omega}_{\mathrm{R}}, \boldsymbol{\Omega}_{\mathrm{T}}) \boldsymbol{\Upsilon}_j(\boldsymbol{\Omega}_{\mathrm{T}}) \mathrm{d}\boldsymbol{\Omega}_{\mathrm{R}} \mathrm{d}\boldsymbol{\Omega}_{\mathrm{T}}. \tag{4}$$

Cluster gains are often defined with a profile (the so-called transition region) where power diminishes at the cluster edges. According to Assumption 2), however, we simplify and assume phase, amplitude gain, and polarization rotation over the opening angles of a cluster to be constant. The error

is assumed negligible for small angular spreads (ASs). Thus, $\boldsymbol{T}_n(\boldsymbol{\Omega}_\mathrm{R}, \boldsymbol{\Omega}_\mathrm{T})$ is constant within the transmit AS,

$$\boldsymbol{T}_n(\boldsymbol{\Omega}_\mathrm{R}, \boldsymbol{\Omega}_\mathrm{T}) = \begin{cases} \boldsymbol{F}_n(\boldsymbol{\Omega}_\mathrm{R}) & \boldsymbol{\Omega}_\mathrm{T} \in \mathcal{D}_n \\ 0 & \boldsymbol{\Omega}_\mathrm{T} \notin \mathcal{D}_n, \end{cases} \tag{5}$$

where $\mathcal{D}_n$ defines the AODs of cluster $n$. Inserting (5) into (4) we get

$$h_{kj} = \sum_{n=0}^{N-1} \int_{4\pi} \boldsymbol{\Psi}_k^\mathrm{H}(\boldsymbol{\Omega}_\mathrm{R}) \boldsymbol{F}_n(\boldsymbol{\Omega}_\mathrm{R}) \Big( \int_{\mathcal{D}_n} \boldsymbol{\Upsilon}_j(\boldsymbol{\Omega}_\mathrm{T}) \mathrm{d}\boldsymbol{\Omega}_\mathrm{T} \Big) \mathrm{d}\boldsymbol{\Omega}_\mathrm{R}. \tag{6}$$

Defining $\overline{\boldsymbol{\Upsilon}}'_{nj}$ as the contribution from BS antenna element $j$ to cluster $n$, we have

$$\begin{aligned} \overline{\boldsymbol{\Upsilon}}'_{nj} &= \int_{\mathcal{D}_n} \boldsymbol{\Upsilon}_j(\boldsymbol{\Omega}_\mathrm{T}) \mathrm{d}\boldsymbol{\Omega}_\mathrm{T} \\ &= \begin{bmatrix} \overline{\boldsymbol{\Upsilon}}^{\Theta}_{nj} e^{j\varphi_{nj}} & 0 \\ 0 & \overline{\boldsymbol{\Upsilon}}^{\Phi}_{nj} e^{j\varphi_{nj}} \end{bmatrix}, \end{aligned} \tag{7}$$

where $\varphi_{nj}$ is the phase offset determined by the antenna geometry in relation to cluster $n$. In (5) we have

$$\boldsymbol{F}_n(\boldsymbol{\Omega}_\mathrm{R}) = \begin{bmatrix} F_n^{\Theta\Theta}(\boldsymbol{\Omega}_\mathrm{R}) & F_n^{\Theta\Phi}(\boldsymbol{\Omega}_\mathrm{R}) \\ F_n^{\Phi\Theta}(\boldsymbol{\Omega}_\mathrm{R}) & F_n^{\Phi\Phi}(\boldsymbol{\Omega}_\mathrm{R}) \end{bmatrix}, \tag{8}$$

which defines the gain, phase, polarization, and the AOAs seen from the terminal receive antennas for cluster $n$. Simplifying the notation, we collect $\boldsymbol{F}_n(\boldsymbol{\Omega}_\mathrm{R}), \forall n$, in a $2 \times 2N$ matrix, $\boldsymbol{F}(\boldsymbol{\Omega}_\mathrm{R}) = [\boldsymbol{F}_0(\boldsymbol{\Omega}_\mathrm{R})\ \boldsymbol{F}_1(\boldsymbol{\Omega}_\mathrm{R}) \cdots \boldsymbol{F}_{N-1}(\boldsymbol{\Omega}_\mathrm{R})]$. We also define $\overline{\boldsymbol{\Upsilon}}$, a $2N \times 2J$ matrix constructed from matrices $\overline{\boldsymbol{\Upsilon}}'_{nj}$, as

$$\overline{\boldsymbol{\Upsilon}} = \begin{bmatrix} \overline{\boldsymbol{\Upsilon}}'_{00} & \cdots & \overline{\boldsymbol{\Upsilon}}'_{0(J-1)} \\ \vdots & \ddots & \vdots \\ \overline{\boldsymbol{\Upsilon}}'_{(N-1)0} & \cdots & \overline{\boldsymbol{\Upsilon}}'_{(N-1)(J-1)} \end{bmatrix}. \tag{9}$$

In matrix notation we now express (6) as,

$$h_{kj} = \Big( \int_{4\pi} \boldsymbol{\Psi}_k^\mathrm{H}(\boldsymbol{\Omega}_\mathrm{R}) \boldsymbol{F}(\boldsymbol{\Omega}_\mathrm{R}) \mathrm{d}\boldsymbol{\Omega}_\mathrm{R} \Big) \overline{\boldsymbol{\Upsilon}}_j, \tag{10}$$

where $\overline{\boldsymbol{\Upsilon}}_j$ denotes one of the $2J$ columns in $\overline{\boldsymbol{\Upsilon}}$.

According to Assumption 3) we consider orthogonal clusters as seen from the BS, i.e., the signal transmitted towards cluster $i$ does not leak to the terminal via any other cluster $j \neq i$. By assuming that clusters, and therefore also E-fields, are non-overlapping as seen from the BS side, $\boldsymbol{E}_{\mathrm{T},i}^\mathrm{H}(\boldsymbol{\Omega}_\mathrm{T}) \boldsymbol{E}_{\mathrm{T},j}(\boldsymbol{\Omega}_\mathrm{T}) = 0$, $i \neq j$ holds and orthogonality is trivially satisfied. Consequences of this assumption are that we neglect energy leakage between clusters and dispersion induced weak signal contributions outside the defined clusters. As the number of BS transmit antenna elements $J$ increases, the angular resolution increases, and the AOD dependency on the phases in the entries of $\overline{\boldsymbol{\Upsilon}}$ makes the different rows asymptotically orthogonal, i.e.

$$\lim_{J \to \infty} \overline{\boldsymbol{\Upsilon}} \overline{\boldsymbol{\Upsilon}}^\mathrm{H} = I. \tag{11}$$

Further simplifying notation, we collect our $K$ terminal antennas in a $K \times 2$ matrix, $\boldsymbol{\Psi}(\boldsymbol{\Omega}) = [\boldsymbol{\Psi}_0(\boldsymbol{\Omega})\ \boldsymbol{\Psi}_1(\boldsymbol{\Omega}) \cdots \boldsymbol{\Psi}_{K-1}(\boldsymbol{\Omega})]^\mathrm{T}$ where all $\boldsymbol{\Psi}_k(\boldsymbol{\Omega})$ are defined with a common center point. Finally, we express the $K \times 2J$ channel transfer function matrix in (1) as

$$\boldsymbol{H} = \Big( \int_{4\pi} \boldsymbol{\Psi}^\mathrm{H}(\boldsymbol{\Omega}) \boldsymbol{F}(\boldsymbol{\Omega}) \mathrm{d}\boldsymbol{\Omega} \Big) \overline{\boldsymbol{\Upsilon}}, \tag{12}$$

where we have removed the subscript R from $\boldsymbol{\Omega}$, as we now only need to consider angles at the terminal side. Note that (12) is valid for any $K$, as long as all antennas are exposed to the same electrical field.

### B. FURTHER SIMPLIFICATION OF THE CHANNEL TRANSFER FUNCTION AND DERIVATION OF AN EXPRESSION FOR THE GRAMIAN

The Gramian, $\boldsymbol{G} = \boldsymbol{H}\boldsymbol{H}^\mathrm{H}$, of a channel transfer function $\boldsymbol{H}$ defines the inner product space for a channel realization. It is well known that system performance depends only on $\boldsymbol{G}$ and not on $\boldsymbol{H}$ itself. Since the Gramian is Hermitian it can be represented by $K(K+1)/2$ numbers. This is much less compared to the full channel matrix which requires $K \times 2J$ numbers. For the special case $K = 2$, a normalized version of the Gramian is reflecting the correlation, $\alpha$, and the power imbalance, $\beta$, between the two terminal receive antennas for a given realization [22],

$$\boldsymbol{G}_\mathrm{N} = \begin{bmatrix} 1+\beta & \alpha \\ \alpha^* & 1-\beta \end{bmatrix}. \tag{13}$$

Invoking our assumptions on the channel properties, we can express $\alpha$ and $\beta$ entirely based on terminal antenna patterns $\boldsymbol{\Psi}(\boldsymbol{\Omega})$ and a limited set of cluster properties. Inserting (12) in (1) we have

$$\boldsymbol{y} = \Big( \int_{4\pi} \boldsymbol{\Psi}^\mathrm{H}(\boldsymbol{\Omega}) \boldsymbol{F}(\boldsymbol{\Omega}) \mathrm{d}\boldsymbol{\Omega} \Big) \overline{\boldsymbol{\Upsilon}} \boldsymbol{x} + \boldsymbol{n}. \tag{14}$$

Provided that $J \geq N$, where each antenna element is represented by two orthogonal polarized antenna ports, we may control phase, amplitude and polarization of the E-field $\boldsymbol{E}_{\mathrm{R}n}(\boldsymbol{\Omega})$ in the direction of each cluster individually (11). By a few manipulations, we can substitute the $2J$ transmit signals with $2N$ signals addressing the respective polarization of the different clusters. To do so, we perform the singular value decomposition (SVD) $\overline{\boldsymbol{\Upsilon}} = \boldsymbol{U}\boldsymbol{S}\boldsymbol{V}^\mathrm{H}$. Multiplying $\overline{\boldsymbol{\Upsilon}}$ with a truncated version of $\boldsymbol{V}$ corresponds to addressing the dominant eigenmodes; the signals $\boldsymbol{x}$ also need to be transformed accordingly. We assign $\boldsymbol{s} = \boldsymbol{V}_\mathrm{eig}^\mathrm{H} \boldsymbol{x}$ and $\boldsymbol{Q} = \overline{\boldsymbol{\Upsilon}} \boldsymbol{V}_\mathrm{eig}$ where $\boldsymbol{V}_\mathrm{eig}$ is the first $2N$ columns of $\boldsymbol{V}$. This gives $\overline{\boldsymbol{\Upsilon}} \boldsymbol{x} = \boldsymbol{U}\boldsymbol{S}\boldsymbol{V}^\mathrm{H}\boldsymbol{x} = \boldsymbol{U}\boldsymbol{S}\boldsymbol{V}^\mathrm{H}\boldsymbol{V}_\mathrm{eig}\boldsymbol{V}_\mathrm{eig}^\mathrm{H}\boldsymbol{x} = \boldsymbol{Q}\boldsymbol{s}$. The input signal $\boldsymbol{s}$ is a $2N \times 1$ vector and $\boldsymbol{V}_\mathrm{eig}$ the precoding matrix generating corresponding signals (i.e. $\boldsymbol{x}$) for the $2J$ antennas, shown to the left in Fig. 2. The matrix $\boldsymbol{Q}$ has a block diagonal structure where each block of size $2 \times 2$ is associated with a cluster.

Equation (14) now becomes

$$\boldsymbol{y} = \Big( \int_{4\pi} \boldsymbol{\Psi}^{\mathrm{H}}(\boldsymbol{\Omega}) \boldsymbol{F}(\boldsymbol{\Omega}) \mathrm{d}\boldsymbol{\Omega} \Big) \boldsymbol{Q}\boldsymbol{s} + \boldsymbol{n}, \tag{15}$$

and the Gramian can be expressed as

$$\boldsymbol{G} = \int_{4\pi} \int_{4\pi} \boldsymbol{\Psi}^{\mathrm{H}}(\boldsymbol{\Omega}_1) \boldsymbol{F}(\boldsymbol{\Omega}_1) \boldsymbol{Q}\boldsymbol{Q}^{\mathrm{H}} \boldsymbol{F}^{\mathrm{H}}(\boldsymbol{\Omega}_2) \boldsymbol{\Psi}(\boldsymbol{\Omega}_2) \mathrm{d}\boldsymbol{\Omega}_1 \mathrm{d}\boldsymbol{\Omega}_2. \tag{16}$$

Orthogonality among rows in $\overline{\boldsymbol{\Upsilon}}$ is maintained also in $\boldsymbol{Q}$, i.e.,

$$\lim_{J \to \infty} \boldsymbol{Q}\boldsymbol{Q}^{\mathrm{H}} = \boldsymbol{I}. \tag{17}$$

With a few more assumptions we are able to simplify (16). Following [20] and [23], and Assumption 4), cluster functions $\boldsymbol{F}_n(\boldsymbol{\Omega})$ are represented by a scalar gain factor multiplied with a unitary matrix, $\boldsymbol{F}_n(\boldsymbol{\Omega}) = \lambda_n \boldsymbol{U}_n(\boldsymbol{\Omega})$. We assume the error caused by this assumption to be small and that it can be assigned to $\lambda_n$, the cluster gain. Here we are interested in how environmental variations impact the number of clusters, their relative power distribution, and the AS (defined as 2 times the angle from the center AOA to the periphery of a circular cluster). We constrain the total power of all clusters for a realization to $N$, hence $\sum_{n=0}^{N-1} \lambda_n^2 = N$. The Gramian can now be expressed

$$\boldsymbol{G} = \sum_{n=0}^{N-1} \lambda_n^2 \int_{4\pi} \int_{4\pi} \boldsymbol{\Psi}^{\mathrm{H}}(\boldsymbol{\Omega}_1) \boldsymbol{U}_n(\boldsymbol{\Omega}_1) \boldsymbol{U}_n^{\mathrm{H}}(\boldsymbol{\Omega}_2) \boldsymbol{\Psi}(\boldsymbol{\Omega}_2) \mathrm{d}\boldsymbol{\Omega}_1 \mathrm{d}\boldsymbol{\Omega}_2. \tag{18}$$

According to Assumption 2) the BS can only resolve a scalar property for each cluster and polarization, $\boldsymbol{U}_n(\boldsymbol{\Omega}_1)\boldsymbol{U}_n^{\mathrm{H}}(\boldsymbol{\Omega}_2) = \boldsymbol{I}$, for the AOA illuminated by each cluster ($\boldsymbol{\Omega}_1, \boldsymbol{\Omega}_2 \in \mathcal{A}_n$), and $\boldsymbol{0}$ otherwise. Thus, each cluster only impacts the amplitude and angular properties at the terminal receive side and the Gramian becomes

$$\boldsymbol{G} = \sum_{n=0}^{N-1} \lambda_n^2 \int_{\mathcal{A}_n} \Big( \int_{\mathcal{A}_n} \boldsymbol{\Psi}^{\mathrm{H}}(\boldsymbol{\Omega}_1) \mathrm{d}\boldsymbol{\Omega}_1 \Big) \boldsymbol{\Psi}(\boldsymbol{\Omega}_2) \mathrm{d}\boldsymbol{\Omega}_2. \tag{19}$$

Simplifying notation further, we define

$$\overline{\boldsymbol{\Psi}}_{k,n} = \int_{\mathcal{A}_n} \boldsymbol{\Psi}_k(\boldsymbol{\Omega}) \mathrm{d}\boldsymbol{\Omega}. \tag{20}$$

and arrive at

$$\boldsymbol{G} = \sum_{n=0}^{N-1} \lambda_n^2 \begin{bmatrix} \overline{\boldsymbol{\Psi}}_{0,n} \\ \overline{\boldsymbol{\Psi}}_{1,n} \end{bmatrix} \begin{bmatrix} \overline{\boldsymbol{\Psi}}_{0,n} & \overline{\boldsymbol{\Psi}}_{1,n} \end{bmatrix}, \tag{21}$$

which, with normalization by the average of diagonal elements, is cast in the form of (13) as

$$\boldsymbol{G}_{\mathrm{N}} = \frac{1}{B} \begin{bmatrix} \sum_{n=0}^{N-1} \lambda_n^2 \left\| \overline{\boldsymbol{\Psi}}_{0,n} \right\|^2 & \sum_{n=0}^{N-1} \lambda_n^2 \overline{\boldsymbol{\Psi}}_{0,n}^{\mathrm{H}} \overline{\boldsymbol{\Psi}}_{1,n} \\ \sum_{n=0}^{N-1} \lambda_n^2 \overline{\boldsymbol{\Psi}}_{1,n}^{\mathrm{H}} \overline{\boldsymbol{\Psi}}_{0,n} & \sum_{n=0}^{N-1} \lambda_n^2 \left\| \overline{\boldsymbol{\Psi}}_{1,n} \right\|^2 \end{bmatrix}, \tag{22}$$

where

$$B = \frac{1}{2} \sum_{n=0}^{N-1} \lambda_n^2 \left( \left\| \overline{\boldsymbol{\Psi}}_{0,n} \right\|^2 + \left\| \overline{\boldsymbol{\Psi}}_{1,n} \right\|^2 \right). \tag{23}$$

We have now reached a point where our communication link is characterized by only a few environment parameters, namely the number of clusters $N$, the cluster gains $\lambda_n$ and their ASs as defined by $\mathcal{A}_n$. Beside those, the simulation framework also uses terminal antenna gain patterns $\boldsymbol{\Psi}_k(\boldsymbol{\Omega})$, see Fig. 1.

### C. ASSIGNING MODEL PARAMETERS

In our simulations, we assume circular clusters uniformly distributed over angle (Assumption 5) with a fixed AS. This assumption is motivated by matching our channel to indoor measurements similar to observations from [24].

However, the measurements in [24] were performed for a limited set of environments, therefore there are no statistical distributions for the propagation delay for the different clusters, and the proposed cluster gain standard deviation, therefore, include effects of both delay and cluster gain. In our simulations, we use the approach in [23], where

$$\lambda_n^2 = N \frac{10^{-D_n/10}}{\sum_{i=0}^{N-1} 10^{-D_i/10}}, \tag{24}$$

and $D_n \sim \mathcal{N}(0, C^2)$ has a Gaussian distribution with mean 0 and standard deviation $C$.

Monte Carlo (MC) simulations are used to calculate empirical distributions of correlation $\alpha$ and power imbalance $\beta$ for the Gramian (22), for various $N$, AS and $C$.

## IV. COMPARISON BETWEEN SIMULATED AND MEASURED PERFORMANCE

We compare free-space (FS) performance with that of beside-head-with-hand-left side (BHHL) in order to analyze in different channel conditions the same environment. The terminal antenna gain patterns are measured patterns of the two top antennas of the Xperia ZL prototype that was used in [9]. The antenna patterns were measured and characterized in an anechoic chamber where a phantom head and a phantom hand were used for the BHHL case, see Fig. 3. Although antenna gain patterns are continuous 2D functions, the measured patterns have 2° resolution in both azimuth and elevation dimensions. We are aware that BHHL is not a typical 5G use case, but its use here is motivated by being well-defined, repeatable, and representing a moderate loading scenario with increased antenna directivity.

### A. ANALYSIS OF PARAMETER IMPACT ON THE GRAMIAN

There are three input parameters that reflect the channel behavior used by the simulation framework, the number of clusters $N$, the cluster gain standard deviation, $C$, and the AS. The impact of the parameters is analyzed through cumulative distribution functions (CDFs) of the Gramian entries,

**FIGURE 3.** Phantom head with hand left.

i.e., $\beta$ and the magnitude of $\alpha$ in (13).[1] In Fig. 4, $|\alpha|$ and $\beta$ are shown as functions of the number of clusters, cluster gain standard deviation and AS.

The leftmost plots of Fig. 4 show CDFs of $|\alpha|$ and $\beta$ as the number of clusters $N$ is changed. Changing $N$ impacts as much on FS as it does on BHHL, as long as $N > 2$, and the CDFs can cover a wide range by adjusting $N$. For the case of a single cluster, the correlation in FS is increased dramatically. In this scenario the correlation is defined by the antenna cross-polarization ratio. The variation of the power imbalance decreases as $N$ grows, while the relative difference between FS and BHHL stays about the same.

The center plots of Fig. 4 show CDFs of $|\alpha|$ and $\beta$ as the cluster gain standard deviation $C$ is altered in the range from 0 to 5 dB. When the cluster gain standard deviation is increased the effective number of clusters is reduced, thus the correlation goes up.

The right upper and lower plots of Fig. 4 show CDFs of $|\alpha|$ and $\beta$, respectively, as the AS is increased from 2° to 48°. For $|\alpha|$ the impact of changing AS is small and affects FS as much as BHHL. This may seem contradictory to the expectation that correlation between antennas decreases as the illuminated angles increases. This, however, is a result of the modeling approach, as we define a single polarization, phase, and amplitude for each cluster in (20), motivated by the fact that the BS is unable to control the signal to each individual MPC. For the power imbalance $\beta$ the AS has an impact on the slope in the BHHL case while the FS curves are shifted in parallel, hence the average power imbalance is reduced. This is due to the constant value of polarization, phase, and amplitude per cluster, which impacts balanced antennas differently.

### B. MEASUREMENT SETUP

Measurements have been performed in an auditorium, as shown in Fig. 5 and Fig. 6. The auditorium was chosen since earlier channel sounding campaigns have been performed in the same place, providing prior knowledge of the channel properties [24]. During all measurements, the MaMi BS was placed in the front center and the terminal in the center of the room. Both the number of clusters and the cluster-power distribution are therefore assumed constant. Additionally, we used an absorbent to block the LOS between the BS and the terminal, mainly due to limitations in the dynamic range of the BHHL measurements. Both FS and BHHL were measured using the same prototype and phantom as during antenna characterization. By only moderately altering the position and rotating the terminal while monitoring channel properties, the variation can be assumed to be determined by the terminal antenna properties in a static propagation channel.

For both FS and BHHL, the terminal was rotated in steps of about 10° for 3 orientations, with a difference in elevation and/or azimuth by 90°. For each load case, 180 channels were measured.

### C. MATCHING THE CHANNELS

To compare simulation and measurement results, $|\alpha|$ and $\beta$ have been computed from the measured Gramian. Then, the Gramians from the measurements and simulations have been matched according to the maximum likelihood (ML) principle, under the assumption that $|\alpha|$ and $\beta$ are independent. Using empirical distributions $\mathrm{Pr}_{\mathrm{scenario}}(\alpha_s)$ and $\mathrm{Pr}_{\mathrm{scenario}}(\beta_s)$ derived from 5000 sample simulations, as described above, we proceed with the parameter estimation. For each set of environmental parameters the product of all probabilities,

$$\mathrm{Pr}_{\mathrm{tot}} = \prod_{s=1}^{S} \left( \mathrm{Pr}_{\mathrm{FS}}(\alpha_s) \mathrm{Pr}_{\mathrm{FS}}(\beta_s) \right) \prod_{v=1}^{V} \left( \mathrm{Pr}_{\mathrm{BHHL}}(\alpha_v) \mathrm{Pr}_{\mathrm{BHHL}}(\beta_v) \right), \tag{25}$$

is calculated, where the number of FS measurements, $S$, is 87 and the number of BHHL measurements, $V$, is 99.

The environmental parameters providing the largest probability were selected and found to be $N = 6$ clusters, AS $= 36°$ and $C = 1$ dB. The cluster gain standard deviation in [24] was between 5 and 6 dB and was estimated based on a set of 14 clusters. In our measurements, we blocked the LOS component which may explain why the cluster gain standard deviation is smaller than that in [24]. It can also be noted that the most influential effect of cluster gain standard deviation is to reduce the effective number of clusters. Hence, increased number of clusters in combination with cluster gain standard deviation yield similar $\mathrm{Pr}_{\mathrm{tot}}$. Fig. 7 shows the CDFs for both measurements and simulations for the selected load cases for $|\alpha|$ and $\beta$ in the upper and lower plots, respectively.

The median and standard deviations of the correlation and power imbalance are shown in Table 1. We note that the medians of the correlation for FS differ by almost a factor of 2, while both correlation and power imbalance for the loaded cases are better captured by the simulation framework.

[1] As we consider only two-antenna terminals, $K = 2$, the corresponding eigenvalues determining performance depend only on the magnitude of off-diagonal elements, $|\alpha|$.

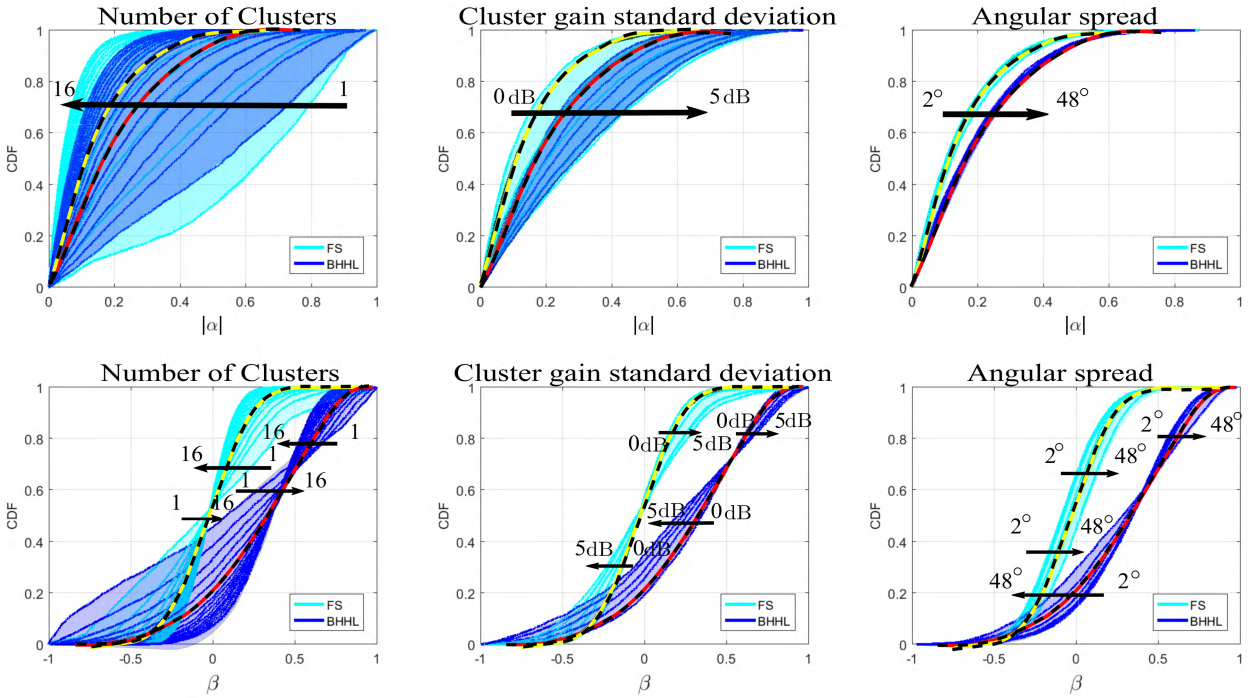


**FIGURE 4.** CDFs of the magnitude of the estimated correlation $\alpha$ (upper row) and power imbalance $\beta$ (lower row). To the left, as a function of the number of clusters, in the center as a function of cluster gain standard deviation, and to the right as a function of AS. The shaded areas highlight the region over which the curves span as a parameter is changed and the highlighted curves are the same in all figures, used as the reference.

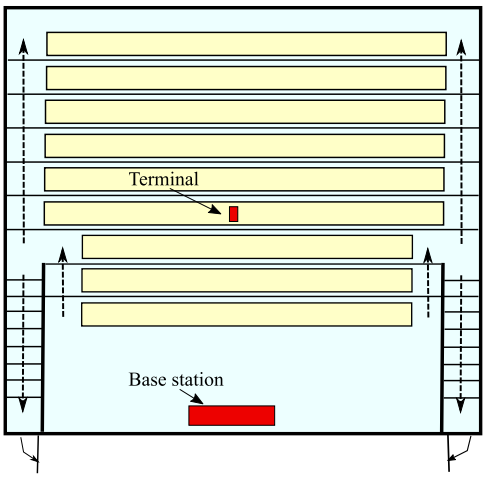


**FIGURE 5.** Overview of the measurement setup in the auditorium.

**FIGURE 6.** A photo showing the measurement setup.

**TABLE 1.** Statistics.

| | Median $\lvert\alpha\rvert$ | STD $\lvert\alpha\rvert$ | Median $\beta$ | STD $\beta$ |
|---|---|---|---|---|
| Sim FS | 0.11 | 0.13 | -0.02 | 0.21 |
| Meas FS | 0.20 | 0.09 | -0.02 | 0.32 |
| Sim BHHL | 0.20 | 0.17 | 0.31 | 0.37 |
| Meas BHHL | 0.16 | 0.22 | 0.21 | 0.43 |

## V. DERIVATION OF RECEIVED SIGNAL PROPERTIES AT THE TERMINAL

While the correlation and power imbalance describe the channel properties, it remains to study their impact on different transmission strategies. Therefore, received signal powers for multi-antenna terminals using the simulation framework are derived next. The three diversity schemes from [9] are implemented and the impact that different pilot transmission strategies have on the received signal will be analyzed. Also, the performance of the different schemes is related to the Gramian (21). Finally, we also introduce a second prototype with a different antenna implementation. We compare the performance of the first and second prototype, using both simulations and measurements.

In all expressions from now on, we assume that the SNR is large so that the noise can be neglected. In section III-B we derived an expression for the received signal at the terminal (14) where we included the cluster based channel model from Fig. 2, still with a dependency on the BS transmit

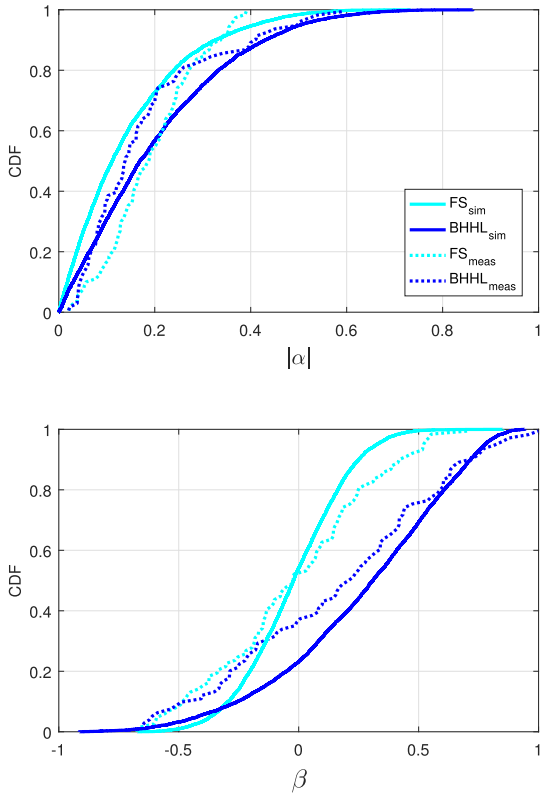


**FIGURE 7.** Estimated magnitude of the correlation $|\alpha|$ (upper) and power imbalance $\beta$ (lower) for measurements and simulations.

antenna elements. In equation (15) we determined the precoding needed to address each cluster individually with a feed vector with $2N$ terms. As we are only interested in the resulting E-field generated by the clusters, we simplify the notation by defining

$$\boldsymbol{\gamma} = \boldsymbol{Q}\boldsymbol{s} \tag{26}$$

from (15) with $2N$ entries $\boldsymbol{\gamma} = [\gamma_0^\Theta \;\; \gamma_0^\Phi \;\; \gamma_1^\Theta \;\; \gamma_1^\Phi \cdots \gamma_{N-1}^\Phi]^{\mathrm{T}}$. Expressing the received signal in terms of $\boldsymbol{\gamma}$-entries we get

$$\boldsymbol{y} = \sum_{n=0}^{N-1} \lambda_n \Big( \int_{4\pi} \boldsymbol{\Psi}^{\mathrm{H}}(\boldsymbol{\Omega}) \boldsymbol{U}_n(\boldsymbol{\Omega}) \mathrm{d}\boldsymbol{\Omega} \Big) \boldsymbol{\gamma}_n, \tag{27}$$

where $\boldsymbol{\gamma}_n = [\gamma_n^\Theta \;\; \gamma_n^\Phi]^{\mathrm{T}}$.

So far, we have assumed full knowledge of the channel at the BS side. In a real TDD MaMi system, the channel is estimated from uplink pilot signals transmitted from the terminal antennas, and the BS use the estimates to optimize $\boldsymbol{\gamma}$. The pilot signal from the terminal determines how the channel is seen by the BS. We assume that the BS blindly performs the same operations based on the received pilot and is not aware of what or which antenna(s) it has been transmitted from. In fact, the BS does not need to know how many antennas the terminal is equipped with. This means that the received signal during the downlink phase at the terminal, in turn, depends on the pilot transmission strategy and that the terminal has some freedom to select this. We define $\boldsymbol{\kappa}$ as the weight vector defining the distribution of the pilot signal to our antennas. For $K$ antennas at the terminal the pilot vector is given by $\boldsymbol{\kappa} = [\kappa_0 \, \kappa_1 \cdots \kappa_{k-1}]^{\mathrm{T}}$, with power which, without loss of generality, is set to $\|\boldsymbol{\kappa}\|^2 = 1$.

Since the assumption is single-antenna terminals, the equivalent effective antenna pattern created by pilots $\boldsymbol{\kappa}$ becomes $\boldsymbol{\Psi}_{\boldsymbol{\kappa}}(\boldsymbol{\Omega}) = \boldsymbol{\kappa}^{\mathrm{T}} \boldsymbol{\Psi}(\boldsymbol{\Omega})$. Further, with this effective antenna pattern, the exploitation of reciprocity leads to an assumed downlink

$$y_{\text{assumed}} = \sum_{n=0}^{N-1} \lambda_n \Big( \int_{4\pi} \boldsymbol{\Psi}_{\boldsymbol{\kappa}}^{\mathrm{H}}(\boldsymbol{\Omega}) \boldsymbol{U}_n(\boldsymbol{\Omega}) \mathrm{d}\boldsymbol{\Omega} \Big) \boldsymbol{\gamma}_n, \tag{28}$$

and the BS optimizes received downlink power as

$$\boldsymbol{\gamma}^{\text{opt}} = \arg \max_{\boldsymbol{\gamma}:\|\boldsymbol{\gamma}\|^2=1} |y_{\text{assumed}}|^2 . \tag{29}$$

This optimization results in $\boldsymbol{\gamma}^{\text{opt}}$ in the form of a spatially matched filter, and thus for cluster $n$ it becomes

$$\boldsymbol{\gamma}_n^{\text{opt}} = \frac{\lambda_n}{q} \int_{4\pi} \boldsymbol{U}_n^{\mathrm{H}}(\boldsymbol{\Omega}) \boldsymbol{\Psi}_{\boldsymbol{\kappa}}(\boldsymbol{\Omega}) \mathrm{d}\boldsymbol{\Omega}, \tag{30}$$

where

$$q = \sqrt{\sum_{n=0}^{N-1} \lambda_n^2 \left\| \int_{4\pi} \boldsymbol{\Psi}_{\boldsymbol{\kappa}}^{\mathrm{H}}(\boldsymbol{\Omega}) \boldsymbol{U}_n(\boldsymbol{\Omega}) \mathrm{d}\boldsymbol{\Omega} \right\|^2} \tag{31}$$

normalizes total cluster power to unity.

Inserting $\boldsymbol{\gamma}_n^{\text{opt}}$ from (30) into (27) and squaring, we express received downlink power on antenna $k$ as

$$P_{k|\boldsymbol{\kappa}} = \frac{1}{q^2 Z_0} \left| \sum_{n=0}^{N-1} \lambda_n^2 \int_{4\pi} \int_{4\pi} \boldsymbol{\Psi}_k^{\mathrm{H}}(\boldsymbol{\Omega}_1) \boldsymbol{U}_n(\boldsymbol{\Omega}_1) \times \boldsymbol{U}_n^{\mathrm{H}}(\boldsymbol{\Omega}_2) \boldsymbol{\Psi}_{\boldsymbol{\kappa}}(\boldsymbol{\Omega}_2) \mathrm{d}\boldsymbol{\Omega}_1 \mathrm{d}\boldsymbol{\Omega}_2 \right|^2, \tag{32}$$

where $Z_0$ is the intrinsic impedance of vacuum ($377\Omega$). Using Assumption 4) and notation from (20), we further simplify to

$$P_{k|\boldsymbol{\kappa}} = \frac{1}{q^2 Z_0} \left| \sum_{n=0}^{N-1} \lambda_n^2 \int_{\mathcal{A}_n} \int_{\mathcal{A}_n} \boldsymbol{\Psi}_k^{\mathrm{H}}(\boldsymbol{\Omega}_1) \boldsymbol{\Psi}_{\boldsymbol{\kappa}}(\boldsymbol{\Omega}_2) \mathrm{d}\boldsymbol{\Omega}_1 \mathrm{d}\boldsymbol{\Omega}_2 \right|^2 \tag{33}$$

$$= \frac{1}{Z_0} \frac{\left| \sum_{n=0}^{N-1} \lambda_n^2 \overline{\boldsymbol{\Psi}}_{k,n}^{\mathrm{H}} \overline{\boldsymbol{\Psi}}_{\boldsymbol{\kappa},n} \right|^2}{\sum_{n=0}^{N-1} \lambda_n^2 \left\| \overline{\boldsymbol{\Psi}}_{\boldsymbol{\kappa},n} \right\|^2}. \tag{34}$$

Like in Section III-B the results from now on are restricted to terminals with two antennas, antenna 0 and antenna 1.

### A. SINGLE ANTENNA TRANSMISSIONS

Assuming that the pilot signal is transmitted from terminal antenna 0 only, using a pilot vector $\boldsymbol{\kappa}_0 = [1\ \ 0]^{\mathrm{T}}$, the received downlink signal on the same antenna is given by (34) as

$$P_{0|\boldsymbol{\kappa}_0} = \frac{1}{Z_0} \sum_{n=0}^{N-1} \lambda_n^2 \left\| \overline{\boldsymbol{\Psi}}_{0,n} \right\|^2. \tag{35}$$

This corresponds to a $Z_0$-scaled version of the first diagonal entry of the Gramian (22), before normalization.

### B. PASSIVE DIVERSITY

Passive diversity (PD) is the case when the terminal has two active receivers, while only a single transmit chain is connected to one of the antennas. This scheme achieves diversity only in the downlink where the received signals from the antennas are combined according to the maximum ratio (MRC) principle. We combine the received signals from both antenna 0, that transmitted the pilot, given by (35), and the leaked signal to antenna 1 given by (34) to get

$$P_{\mathrm{PD}|\boldsymbol{\kappa}_0} = P_{0|\boldsymbol{\kappa}_0} + P_{1|\boldsymbol{\kappa}_0}, \tag{36}$$

where

$$P_{1|\boldsymbol{\kappa}_0} = \frac{1}{Z_0} \frac{\left| \sum_{n=0}^{N-1} \lambda_n^2 \overline{\boldsymbol{\Psi}}_{1,n}^{\mathrm{H}} \overline{\boldsymbol{\Psi}}_{0,n} \right|^2}{\sum_{n=0}^{N-1} \lambda_n^2 \left\| \overline{\boldsymbol{\Psi}}_{0,n} \right\|^2}. \tag{37}$$

As the expression indicates, the leaked signal to antenna 1 depends mainly on the off-diagonal entries of the Gramian (34).

By transmitting a pilot signal from each antenna, on different time-frequency resources, the terminal can compute the magnitude of the different entries in the Gramian from the received signals.

### C. SWITCHED DIVERSITY

In switched diversity (SWD), the terminal antenna giving the highest received downlink power is always selected for all transmissions. For each cluster scenario, we need to optimize $\boldsymbol{\gamma}$ for both antennas and select the $\boldsymbol{\gamma}$ and the associated antenna that yields the highest power. This means

$$P_{\mathrm{SWD}} = \max\left(P_{0|\boldsymbol{\kappa}_0}, P_{1|\boldsymbol{\kappa}_1}\right), \tag{38}$$

where $\boldsymbol{\kappa}_1 = [0\ \ 1]$, and from (35) we get

$$P_{0|\boldsymbol{\kappa}_0} = \frac{1}{Z_0} \sum_{n=0}^{N-1} \lambda_n^2 \left\| \overline{\boldsymbol{\Psi}}_{0,n} \right\|^2, \tag{39}$$

and

$$P_{1|\boldsymbol{\kappa}_1} = \frac{1}{Z_0} \sum_{n=0}^{N-1} \lambda_n^2 \left\| \overline{\boldsymbol{\Psi}}_{1,n} \right\|^2. \tag{40}$$

Again we see that the Gramian (21) reveals the achieved performance. This time through its largest diagonal entry.

### D. DOMINANT EIGENMODE

Dominant eigenmode (DEM) is when both terminal antennas are used simultaneously for all transmissions in an SNR-optimal way. Based on our framework the BS needs to determine the $\boldsymbol{\gamma}$ that maximizes received power, i.e.

$$\boldsymbol{\gamma}^{\mathrm{opt}} = \arg \max_{\boldsymbol{\gamma}:\|\boldsymbol{\gamma}\|^2=1} \left( |y_0|^2 + |y_1|^2 \right). \tag{41}$$

In an idealized noise-free case, the channel $\boldsymbol{H}$ based on (27) is given by,

$$\boldsymbol{H} = \sum_{n=0}^{N-1} \lambda_n \int_{4\pi} \boldsymbol{\Psi}^{\mathrm{H}}(\boldsymbol{\Omega}) \boldsymbol{U}_n(\boldsymbol{\Omega}) \mathrm{d}\boldsymbol{\Omega}. \tag{42}$$

With $\boldsymbol{y} = \boldsymbol{H}\boldsymbol{\gamma}$, the constrained maximization in (41) becomes,

$$\boldsymbol{\gamma}^{\mathrm{opt}} = \underset{\boldsymbol{\gamma}}{\mathrm{argmax}} \left( \frac{\boldsymbol{\gamma} \boldsymbol{H}^{\mathrm{H}} \boldsymbol{H} \boldsymbol{\gamma}}{\boldsymbol{\gamma}^{\mathrm{H}} \boldsymbol{\gamma}} \right). \tag{43}$$

To maximize (43), $\boldsymbol{\gamma}$ is selected as the eigenvector associated with the largest eigenvalue of $\boldsymbol{H}^{\mathrm{H}}\boldsymbol{H}$. This requires that the BS knows $\boldsymbol{H}$. But, the BS automatically finds $\boldsymbol{\gamma}^{\mathrm{opt}}$ if the terminal weight the pilot signals with the eigenvector associated with the strongest eigenvalue of the Gramian, defined as $\boldsymbol{\kappa}^{\mathrm{opt}} = \boldsymbol{v}_1(\boldsymbol{G})$. This follows from the fact that the inner and outer product have the same eigenvalues, $\mathrm{eig}(\boldsymbol{H}^{\mathrm{H}}\boldsymbol{H}) = \mathrm{eig}(\boldsymbol{H}\boldsymbol{H}^{\mathrm{H}})$, where the latter is $\mathrm{eig}(\boldsymbol{G})$.

We use the same weight vector for the received signals at the terminal by multiplying (27) with $\boldsymbol{\kappa}^{\mathrm{opt}}$ and

$$y_{\mathrm{DEM}} = (\boldsymbol{\kappa}^{\mathrm{opt}})^{\mathrm{T}} \boldsymbol{y}_{|\boldsymbol{\kappa}^{\mathrm{opt}}}.$$

Following (32)-(34), the received power becomes

$$P_{\mathrm{DEM}} = \frac{1}{Z_0} \sum_{n=0}^{N-1} \lambda_n^2 \left\| \overline{\boldsymbol{\Psi}}_{\boldsymbol{\kappa},n}(\boldsymbol{\Omega}) \right\|^2. \tag{44}$$

If we select the weight vector $\boldsymbol{\kappa}_0$ in (44) we get $P_{0|\boldsymbol{\kappa}_0}$ from (35) and similarly the selection of $\boldsymbol{\kappa}_1$ yields $P_{1|\boldsymbol{\kappa}_1}$.

Deriving the DEM performance from the Gramian (21) is a bit more involved than for the other schemes. The DEM performance is given by

$$P_{\mathrm{DEM}} = \frac{1}{Z_0} (\boldsymbol{v}_1 |\boldsymbol{G}|)^{\mathrm{T}} |\boldsymbol{G}| [1\ \ 1]^{\mathrm{T}}, \tag{45}$$

where $|\cdot|$ denotes the magnitude of the matrix entries. Given the diversity schemes above, we can evaluate their performance for different terminal antenna configurations and pilot transmission strategies in the context of a MaMi by MC simulations. For this we need to select appropriate values on the AS, the number of clusters $N$ and the cluster gain standard deviation $C$, matching the targeted propagation environment.

Table 2 presents a summary of pilot vectors, $\boldsymbol{\gamma}^{\mathrm{opt}}$, received powers, and how they relate to the Gramian, for the different schemes. It can be argued that a pilot needs to be transmitted from each terminal antenna in order to determine the Gramian, i.e. $\boldsymbol{\kappa}_0$ and $\boldsymbol{\kappa}_1$, before the weight vector for SWD

**TABLE 2. Terminal pilot strategies, Power and Gramian relation for a 2 antenna terminal.**

| Mode | Pilot vector | Received power | Gramian relation | |
|---|---|---|---|---|
| Single | $\boldsymbol{\kappa}_0$ | $P_{0\|\boldsymbol{\kappa}_0}$ | $\boldsymbol{\kappa}_0^{\mathrm{T}}\boldsymbol{G}\boldsymbol{\kappa}_0$ | |
| Leaked | $\boldsymbol{\kappa}_0$ | $P_{1\|\boldsymbol{\kappa}_0}$ | $\boldsymbol{\kappa}_0^{\mathrm{T}}\boldsymbol{G}\boldsymbol{\kappa}_1$ | |
| PD | $\boldsymbol{\kappa}_0$ | $P_{0\|\boldsymbol{\kappa}_0}+P_{1\|\boldsymbol{\kappa}_0}$ | $\boldsymbol{\kappa}_0^{\mathrm{T}}\|\boldsymbol{G}\|[1\ 1]^{\mathrm{T}}$ | |
| SWD | $\boldsymbol{\kappa}_0$ or $\boldsymbol{\kappa}_1$ | $\max(P_{0\|\boldsymbol{\kappa}_0}, P_{1\|\boldsymbol{\kappa}_1})$ | $\max(\boldsymbol{\kappa}_0^{\mathrm{T}}\boldsymbol{G}\boldsymbol{\kappa}_0, \boldsymbol{\kappa}_1^{\mathrm{T}}\boldsymbol{G}\boldsymbol{\kappa}_1)$ | |
| DEM | $\boldsymbol{\kappa}^{\mathrm{opt}}$ | $P_{\boldsymbol{\kappa}^{\mathrm{opt}}\|\boldsymbol{\kappa}^{\mathrm{opt}}}$ | $(\boldsymbol{\kappa}^{\mathrm{opt}})^{\mathrm{T}}\|\boldsymbol{G}\|[1\ 1]^{\mathrm{T}}$ | |

or DEM can be computed. For this evaluation, however, we assume that they are available. This corresponds to slow-enough changes in the channel for them to be appropriately estimated.

## VI. PROTOTYPE TERMINAL SIMULATION RESULTS

In this section, we present results based on MC simulations where the different transmission strategies are examined. In order to evaluate the framework, we compare the SNR gains for the different transmission schemes from simulations and measurements. In the simulations, we have applied the settings described in Section IV-C. Finally, to evaluate the validity of the environmental parameters, we introduce a second prototype, simulate it with the same settings, and compare the SNR gains to measured values.

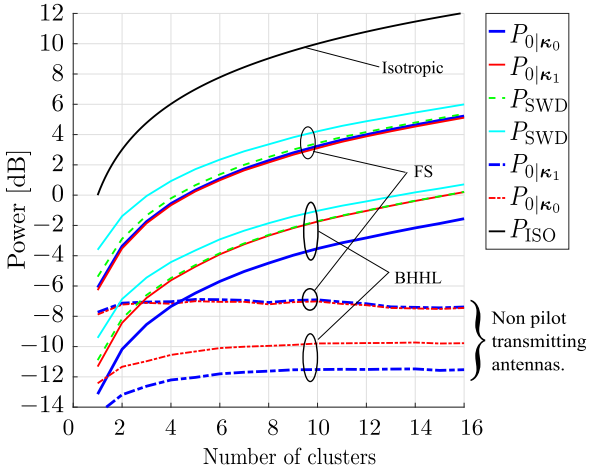


**FIGURE 8. Simulated sample means for received powers $P_{0|\kappa_0}$, $P_{1|\kappa_1}$, $P_{\mathrm{SWD}}$, $P_{\mathrm{DEM}}$, $P_{0|\kappa_1}$, and $P_{0|\kappa_1}$ for FS and BHHL, as functions of the number of clusters, $N$, at the terminal side. Received power $P_{\mathrm{ISO}}$ for an isotropic radiator (top curve) is shown as reference.**

Fig. 8 shows sample means for received powers $P_{0|\kappa_0}$, $P_{1|\kappa_1}$, $P_{\mathrm{SWD}}$, $P_{\mathrm{DEM}}$, $P_{0|\kappa_1}$, and $P_{0|\kappa_1}$, as functions of the number of clusters at the terminal side. Power on the vertical axis is normalized to that of an isotropic radiator with gain 0 dB, $P_{\mathrm{ISO}}$ in Fig. 8, when a single cluster is present. For single antenna transmission (35), the expected power at $n = 1$ equals the total radiated power in an isotropic environment. In this case, the received power grows with the number of clusters $n$, and the slope is limited by the directive gain of the antenna and the cluster gain standard deviation.

The powers in the figure are computed for a cluster AS of 36° and a cluster-gain standard deviation $C$ of 1 dB as

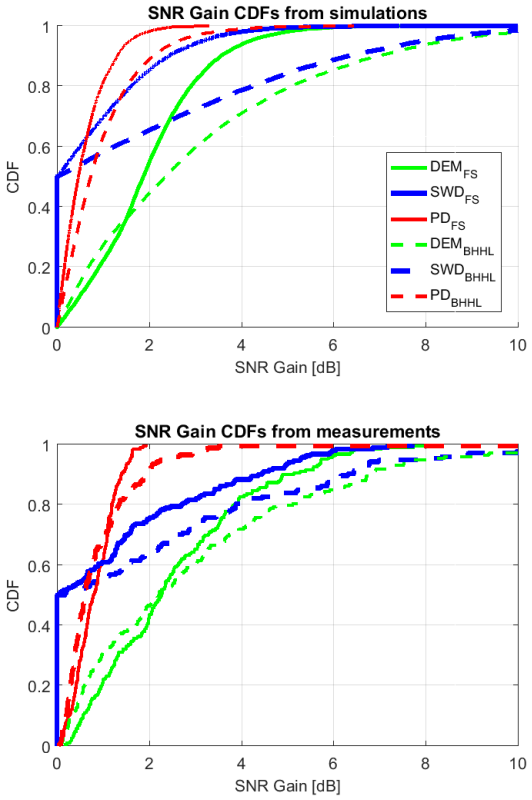


**FIGURE 9. CDFs of SNR gains for the Xperia ZL prototype for the different diversity schemes. Simulation results above and measurement results below.**

we derived in Section IV-C. The upper curves are for FS condition and the lower curves are for BHHL condition. We can clearly see that the power received by the non-pilot transmitting antennas, e.g. $P_{0|\kappa_1}$ and $P_{1|\kappa_0}$, do not benefit from increased number of clusters. The offset between the FS curves and the BHHL curves shows the drop in efficiency caused by loading the antennas, BHHL load degrades power by 7 dB for antenna 0 and 5 dB for antenna 1.

With DEM we observe a significant increase in the received power, about 1 dB higher average power than the average power received by the better antenna can be expected. For SWD the average received power is slightly higher than the average power of the best performing antenna. PD powers are not included in Fig. 8 for clarity. It can, however, be mentioned that the power for PD is close to the performance for the respective antenna, especially when the number of clusters increases and the ratio $P_{0|\kappa_0}/P_{1|\kappa_0}$ or $P_{1|\kappa_1}/P_{0|\kappa_1}$ becomes large. The different diversity schemes have been implemented in the LuMaMi [10], [11] testbed and measurements have been performed with the same setup as described in section IV-B. As it is not possible to sweep the number of clusters in measurements, we examine the distribution, i.e. the CDF, for $N = 6$ clusters as described in Section IV-C. By looking at the relative SNR gain obtained for the different transmission schemes compared to that of a single antenna the result become independent on the absolute power level. This enables a direct comparison to measurements.

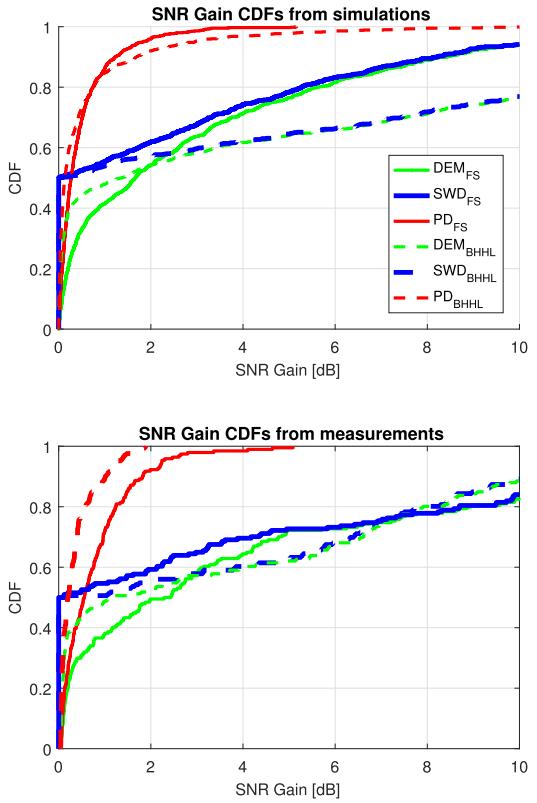


**FIGURE 10.** CDFs of the SNR gains for a second prototype, Xperia SP, for the different diversity schemes. Simulation results above and measurement results below.

Fig. 9 shows the CDFs of simulated (top) and measured (bottom) SNR gains [9], i.e. the CDFs of the relative improvements in SNR achieved by a diversity scheme compared to that of a single antenna. Both antennas have been used as the reference in the plots and this explains why the SWD curves start at 0.5. The plots indicate the improvement that can be expected if a second antenna is added to a MaMi terminal. SNR gain CDFs are shown for DEM, SWD, and PD, for both FS and BHHL. Channel dependent parameters in the simulations are set according to section IV-C.

We conclude that the behavior of the simulated SNR gains is similar to the measured ones, with larger values in the BHHL case for all schemes. The SNR gain is slightly underestimated in the simulations in the FS case and overestimated in the BHHL case. A possible explanation for this discrepancy is related to the fact that the BHHL loading is hard to repeat with full accuracy. A slight change in the terminal position in the hand may cause a large difference in the loading profile.

To further evaluate our approach the second prototype, with a different antenna configuration based on an Xperia SP smartphone, is examined. The results are presented in Fig. 10. Environmental settings for the simulations and the measurement environment are the same as those used with the Xperia ZL prototype. The antennas in the Xperia SP prototype are mounted in the top and bottom of the chassis. In FS condition the antennas are unbalanced by about 3 dB and the gain patterns show a directive gain in opposite directions, which is reflected in the results by larger SNR gains for the SWD and DEM schemes when compared to the results for the Xperia ZL prototype. A low correlation between antennas is indicated by the sharp slope in the beginning of the DEM curves and this is captured well both by simulations and measurements. For this reason, the DEM scheme often directs all power to only one of the antennas and DEM performance tend to be similar to that of SWD.

We conclude that the influence of different antenna properties and loading effects are well captured by the simulation framework. The behavior of the different diversity schemes and pilot transmission strategies are also nicely captured. We further conclude that the limited number of parameters we use to model the channel yields good predictions of the antenna performance for the tested environment.

## VII. SUMMARY

We have presented a simulation framework for the evaluation of the behavior of terminal antennas in a precoded MaMi system. The simulation framework randomly generates clusters with properties relevant for such MaMi channels. By ML estimation of the number of clusters, the cluster gain, and the angular spread we have shown that the proposed simulation framework can predict the behavior of different terminal antenna designs and loading effects in an indoor environment. The channel dependent parameters have been determined based on mapping of the CDFs for the antenna correlation and power imbalance to a real measured channel.

With the presented simulation framework, it is possible to evaluate terminal antenna designs, directional properties, loading effects and diversity schemes that take the pilot transmission strategies into account in a MaMi context, without performing extensive and time-consuming simulations of complicated base station processing and detailed channel models. This study is performed at 3.7 GHz. We believe that the simulation framework can be used also in a wider frequency range and in other environments, with appropriate selection of the parameters. We have, however, no results to back this up and consider it as an area for further study. At higher frequencies, above 6 GHz, some of the assumptions may need to be changed and also the transmission strategies may need to be changed accordingly.

## ACKNOWLEDGMENT

The authors would like to thank the anonymous reviewers for their valuable comments.

## REFERENCES

[1] T. L. Marzetta, "Noncooperative cellular wireless with unlimited numbers of base station antennas," *IEEE Trans. Wireless Commun.*, vol. 9, no. 11, pp. 3590–3600, Nov. 2010. [Online]. Available: http://dx.doi.org/10.1109/TWC.2010.092810.091092

[2] E. G. Larsson, O. Edfors, F. Tufvesson, and T. L. Marzetta, "Massive MIMO for next generation wireless systems," *IEEE Commun. Mag.*, vol. 52, no. 2, pp. 186–195, Feb. 2014. [Online]. Available: http://dx.doi.org/10.1109/MCOM.2014.6736761

[3] H. Q. Ngo, E. G. Larsson, and T. L. Marzetta, "Energy and spectral efficiency of very large multiuser MIMO systems," *IEEE Trans. Commun.*, vol. 61, no. 4, pp. 1436–1449, Apr. 2013. [Online]. Available: http://dx.doi.org/10.1109/TCOMM.2013.020413.110848

[4] A. Nordrum, "5G researchers set new world record for spectrum efficiency," *IEEE Spectr.*, May 2016. [Online]. Available: http://spectrum.ieee.org/tech-talk/telecom/wireless/5g-researchers-achieve-new-spectrum-efficiency-record

[5] *Study on Scenarios and Requirements for Next Generation Access Technologies*, document TR 38.913, ETSI, 3GPP, 2017.

[6] *Study on New Radio (NR) Access Technology*, document TR 38.912, ETSI, 3GPP, 2017.

[7] E. Björnson, J. Hoydis, M. Kountouris, and M. Debbah, "Massive MIMO systems with non-ideal hardware: Energy efficiency, estimation, and capacity limits," *IEEE Trans. Inf. Theory*, vol. 60, no. 11, pp. 7112–7139, Nov. 2014. [Online]. Available: http://dx.doi.org/10.1109/TIT.2014.2354403

[8] E. L. Bengtsson, F. Tufvesson, and O. Edfors, "UE antenna properties and their influence on massive MIMO system performance," in *Proc. 9th Eur. Conf. Antennas Propag. (EUCAP)*, Lisbon, Portugal, Apr. 2015, pp. 1–5.

[9] E. L. Bengtsson *et al.*, "Transmission schemes for multiple antenna terminals in real massive MIMO system," in *Proc. IEEE Commun. Soc. GlobeCom Conf.*, Washington, DC, USA, Dec. 2016, pp. 1–6.

[10] J. Vieira *et al.*, "A flexible 100-antenna testbed for massive MIMO," in *Proc. Globecom Workshops (GC Wkshps)*, 2014, pp. 287–293.

[11] S. Malkowsky *et al.*, "wall, and O. Edfors, "Real-time testbed for massive MIMO: Design, implementation, and real-life validation," *IEEE Access*, pp. 9073–9088, May 2017.

[12] B. Clerckx and C. Oestges, *MIMO Wireless Networks*, 2nd ed. San Francisco, CA, USA: Academic, 2013.

[13] X. Gao, O. Edfors, F. Rusek, and F. Tufvesson, "Linear pre-coding performance in measured very-large MIMO channels," in *Proc. 74th IEEE Veh. Technol. Conf.*, Sep. 2011, pp. 1–5.

[14] X. Gao, O. Edfors, F. Rusek, and F. Tufvesson, "Massive MIMO performance evaluation based on measured propagation data," *IEEE Trans. Wireless Commun.*, vol. 14, no. 7, pp. 3899–3911, Jul. 2015. [Online]. Available: http://dx.doi.org/10.1109/TWC.2015.2414413

[15] J. Flordelis, X. Gao, G. Dahman, F. Rusek, O. Edfors, and F. Tufvesson, "Spatial separation of closely-spaced users in measured massive multi-user MIMO channels," in *Proc. IEEE Int. Conf. Commun. (ICC)*, Jun. 2015, pp. 1441–1446. [Online]. Available: http://dx.doi.org/10.1109/ICC.2015.7248526

[16] X. Gao, J. Flordelis, G. Dahman, F. Tufvesson, and O. Edfors, "Massive MIMO channel modeling—Extension of the COST 2100 model," in *Proc. Joint NEWCOM/COST Workshop Wireless Commun. (JNCW)*, Barcelona, Spain, 2015. [Online]. Available: https://www.semanticscholar.org/paper/Massive-MIMO-Channel-Modeling-Extension-of-the-COS-Gao-Flordelis/0ca36e2da6e985e3979e0f8f7f6e58f8867a1800

[17] A. Alayon Glazunov, A. Molisch, and F. Tufvesson, "Mean effective gain of antennas in a wireless channel," *IEEE Antennas Propag.*, vol. 2, pp. 214–227, Feb. 2009.

[18] K. Zhao, E. Bengtsson, Z. Ying, and S. He, "Multiplexing efficiency of high order MIMO in mobile terminal in different propagation scenarios," in *Proc. 10th Eur. Conf. Antennas Propag. (EuCAP)*, Apr. 2016, pp. 1–4.

[19] B. M. Hochwald, T. L. Marzetta, and V. Tarokh, "Multiple-antenna channel hardening and its implications for rate feedback and scheduling," *IEEE Trans. Inf. Theory*, vol. 50, no. 9, pp. 1893–1909, Sep. 2004. [Online]. Available: http://dx.doi.org/10.1109/TIT.2004.833345

[20] R. Verdone and A. Zanella, *Pervasive Mobile and Ambient Wireless Communications*. Lindon, UT, USA: Springer-Verlag, 2012.

[21] P. Kyösti, J. Meinilä, and L. Hentilä, *WINNER II Channel Models*. 2007. [Online]. Available: https://cept.org/files/8339/winner2%20-%20final%20report.pdf

[22] X. Gao, F. Tufvesson, O. Edfors, and F. Rusek, "Measured propagation characteristics for very-large MIMO at 2.6 GHz," in *Proc. Conf. Rec. 46th Asilomar Conf. Signals, Syst. Comput. (ASILOMAR)*, Nov. 2012, pp. 295–299.

[23] *Universal Mobile Telecommunications System (UMTS) Spatial Channel Model for Multiple Input Multiple Output (MIMO) Simulations*, document TR 25.996, ETSI, 3GPP, 2014.

[24] B. Clerckx and C. Oestges, "D1.2 MaMi channel characteristics: Measurement results," MAMMOET, Schiedam, The Netherlands, Tech. Rep. 619086, Jun. 2015.


**ERIK L. BENGTSSON** received the M.Sc. degree in electrical engineering from Lund University 1997. He joined Ericsson Mobile Communication AB, Lund, the same year and worked with the RF ASIC design until 2005. He then joined Nokia A/S, Copenhagen, and worked with the antenna concept development with a focus on reconfigurable antennas. In 2011, he joined Sony Mobile, Lund, and belongs to the Radio Access Lab. Since 2015, he has been an Industry Ph.D. Student with the Department of Electrical and Information Technology, Lund University, partly funded by the Swedish Foundation for Strategic Research. His current research focus is terminal diversity aspects from a massive MIMO perspective.

**FREDRIK RUSEK** was born in Lund, Sweden, in 1978. He received the M.S. and Ph.D. degrees in electrical engineering from Lund University, Lund, in 2003 and 2007, respectively. Since 2012, he has held an Associate Professorship with the Department of Electrical and Information Technology, Lund Institute of Technology. From 2012 to 2014, he held an algorithm researcher position with Huawei, Lund. His research interests include modulation theory, equalization, wireless communications, and applied information theory.

**STEFFEN MALKOWSKY** received the B.Eng. degree in electrical engineering and information technology from Pforzheim University, Germany, in 2011, and the M.Sc. degree in electronic design from Lund University in 2013, where he is currently pursuing the Ph.D. degree with the Digital ASIC Group, Department of Electrical and Information Technology. His research interests include the development of reconfigurable hardware and implementation of algorithms for wireless communication with an emphasis on massive MIMO. For the development of a massive MIMO testbed in collaboration with the University of Bristol and National Instruments and a set spectral efficiency world record, he received five international awards from National Instruments, Xilinx, and Hewlett Packard Enterprise.

**FREDRIK TUFVESSON** (F'17) received the Ph.D. degree from Lund University, Sweden, in 2000. After two years at a startup company, he joined the Department of Electrical and Information Technology, Lund University, where he is currently a Professor of radio systems. His main research interests are the interplay between the radio channel and the rest of the communication system with various applications in 5G systems, such as massive MIMO, mm-wave communication, vehicular communication, and radio-based positioning. He has authored around 65 journal papers and 130 conference papers. He received the Neal Shepherd Memorial Award for the best propagation paper in the IEEE TRANSACTIONS ON VEHICULAR TECHNOLOGY.

**PETER C. KARLSSON** received the Ph.D. degree in applied electronics from the Lund Institute of Technology in 1995, with a thesis on indoor radio wave propagation. He joined Telia Research and had different research and management positions in the wireless and mobile communications systems area. In 2000, he had a one year post-doctoral position and research fellow position at the Center for Communications Research, University of Bristol. He joined Sony Ericsson corporate technology office in 2007. He was leading the Network Technology Lab with the new Sony Mobile organization in 2012. He is currently the Head of the Research and Standardisation Department, Sony Mobile, Research and Incubation, Lund focusing on 5G and IoT topics. He has authored and co-authored some 75 conference and journal papers in the mobile and wireless communications area.

**OVE EDFORS** is currently a Professor of radio systems with the Department of Electrical and Information Technology, Lund University, Sweden. His research interests include statistical signal processing and low-complexity algorithms with applications in wireless communications. In the context of massive MIMO, his research focus is on how realistic propagation characteristics influence system performance and baseband processing complexity.